Engineering Geology 116 (2010) 184–188

Contents lists available at ScienceDirect

Engineering Geology

journal homepage: www.elsevier.com/locate/enggeo

Technical note

# Liquefaction caused by the 2009 Olancha, California (USA), *M*5.2 earthquake

Thomas L. Holzer [a,*], Angela S. Jayko [b], Egill Hauksson [c], Jon P.B. Fletcher [a], Thomas E. Noce [a], Michael J. Bennett [a], Christopher M. Dietel [a], Kenneth W. Hudnut [d]

[a] U.S. Geological Survey (MS977), 345 Middlefield Road, Menlo Park, CA 94025, USA
[b] U.S. Geological Survey, U.C. White Mountain Research Station, 3000 East Line Street, Bishop, CA 93514, USA
[c] Division of Geological and Planetary Sciences (MC 252-21), California Institute of Technology, Pasadena, CA 91125, USA
[d] U.S. Geological Survey, 525 South Wilson Avenue, Pasadena, CA 91106, USA

ARTICLE INFO

*Article history:*
Received 16 January 2010
Received in revised form 8 July 2010
Accepted 14 July 2010
Available online 29 July 2010

*Keywords:*
Liquefaction
Earthquake
Simplified procedure
Paleoliquefaction

ABSTRACT

The October 3, 2009 (01:16:00 UTC), Olancha *M*5.2 earthquake caused extensive liquefaction as well as permanent horizontal ground deformation within a 1.2 km$^2$ area earthquake in Owens Valley in eastern California (USA). Such liquefaction is rarely observed during earthquakes of $M \leq 5.2$. We conclude that subsurface conditions, not unusual ground motion, were the primary factors contributing to the liquefaction. The liquefaction occurred in very liquefiable sands at shallow depth (<2 m) in an area where the water table was near the land surface. Our investigation is relevant to both geotechnical engineering and geology. The standard engineering method for assessing liquefaction potential, the Seed–Idriss simplified procedure, successfully predicted the liquefaction despite the small earthquake magnitude. The field observations of liquefaction effects highlight a need for caution by earthquake geologists when inferring prehistoric earthquake magnitudes from paleoliquefaction features because small magnitude events may cause such features.

Published by Elsevier B.V.

## 1. Introduction

Liquefaction is the loss of strength and stiffness of saturated loose sand caused by pore-water pressure buildup as the sand contracts when shaken. It is common in earthquakes with moment magnitudes (*M*) greater than 6 and frequently causes damage, but it is rarely associated with earthquakes of $M \leq 5.2$. In fact, descriptions of liquefaction have been published for only four earthquakes with instrumentally determined $M \leq 5.2$ (Kuribayashi and Tatsuoka, 1975; Ambraseys, 1988; Sims and Garvin, 1995; Galli, 2000). None of these occurrences have been comprehensively studied from both geological and geotechnical perspectives. The smallest event, and the only one for which liquefaction was mapped and described in detail, is an *M*4.6 aftershock of the 1989 Loma Prieta, California, earthquake (Sims and Garvin, 1995). It liquefied very susceptible sediments in a nearby tailings pond. (After submission of this manuscript, it was brought to the authors attention that the April 15, 2010, Randolph, Utah, *M*4.6 earthquake caused liquefaction of alluvial deposits along a 1 km stretch of the Bear River (C.B. DuRoss, pers. comm., 2010)) Our report documents an unusual occurrence of liquefaction of natural sediments caused by a small magnitude earthquake, the October 3, 2009 (01:16:00 UTC), Olancha, California, *M*5.2 earthquake (Fig. 1), and assesses how well current engineering practice predicts its occurrence.

Observations of liquefaction at very small earthquake magnitudes have application to both geotechnical engineering and geology. For geotechnical engineering, these observations provide guidance on the threshold magnitude at which liquefaction potential should be considered in practice. Databases (Cetin et al., 2004; Moss et al., 2006) that are used by engineers to support the primary empirical procedures for predicting liquefaction (Seed and Idriss, 1971) include only one earthquake with $M < 6$, the 1981 *M*5.9 Westmorland, California, earthquake. In addition, the database on which many predictions of liquefaction-induced horizontal displacements are based contains no earthquakes with $M < 6.4$ (Youd et al., 2002). Thus, none of these databases provide empirical guidance to establish lower magnitude bounds for engineering design. For geology, the observation of liquefaction during small magnitude earthquakes provides a threshold magnitude at which liquefaction features might be generated in the field. Earthquake geologists often use paleoliquefaction features exposed in excavations across active faults to recognize and date prehistoric earthquakes. Geologists may even rely exclusively on paleoliquefaction features to identify prehistoric earthquakes in areas where active faults are not exposed at the land surface (Obermeier et al., 2005).

## 2. Olancha earthquake

The 2009 Olancha *M*5.2 earthquake was part of an earthquake swarm that was located in eastern California between the northeast edge of the Coso Range and the southwest edge of Owens Valley

* Corresponding author. Tel.: +1 650 329 5637; fax: +1 650 329 5163.
*E-mail address:* tholzer@usgs.gov (T.L. Holzer).

0013-7952/$ – see front matter. Published by Elsevier B.V.
doi:10.1016/j.enggeo.2010.07.009

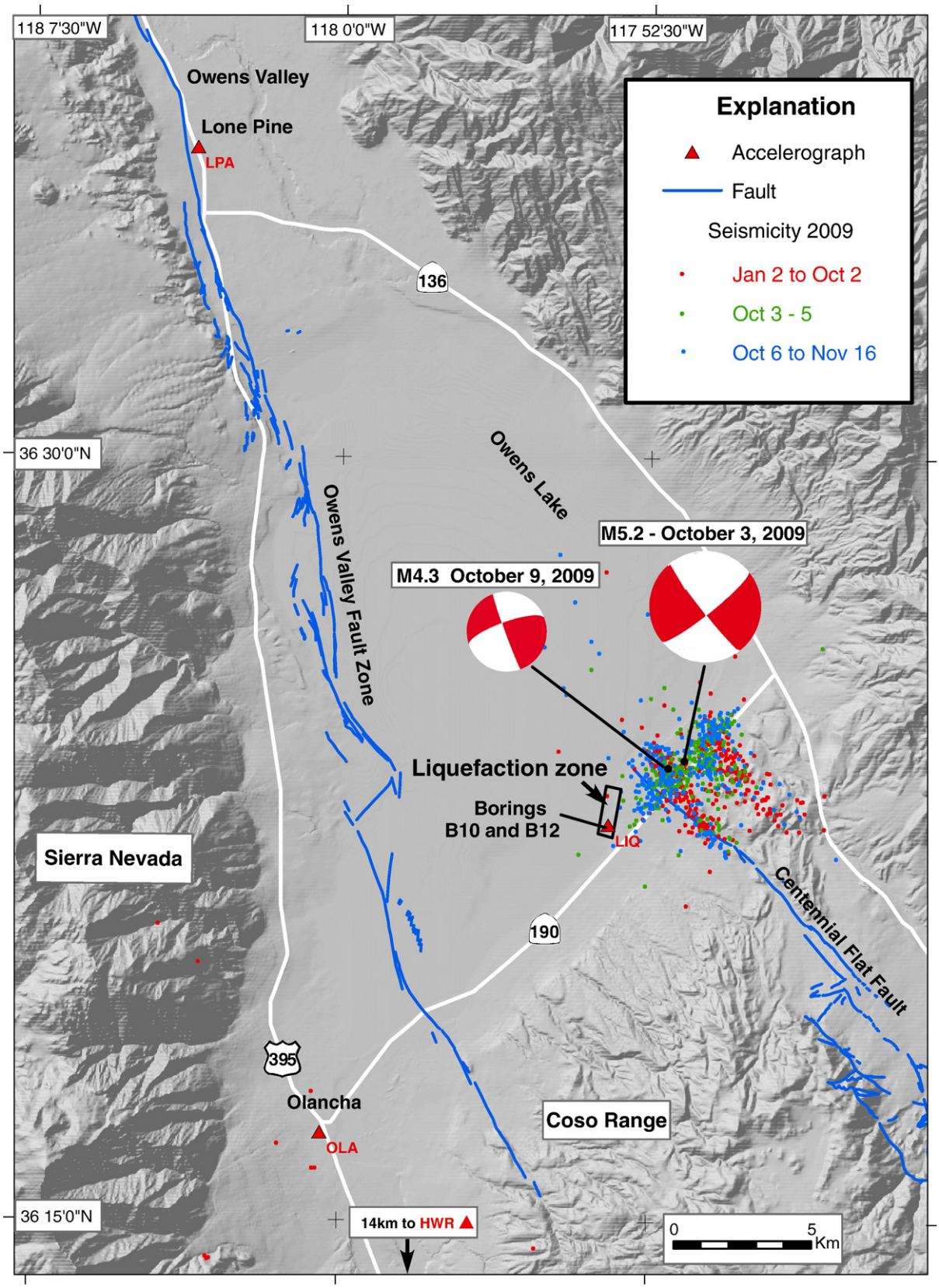


**Fig. 1.** Map of Owens Valley, California (USA), showing liquefaction zone caused by the October 3, 2009 (01:16:00 UTC), Olancha *M*5.2 earthquake. Dots show epicenters of the earthquake swarm, colored by indicated date interval. Red and white "beach ball" symbols show fault plane solutions, i.e., orientation of nodal planes and direction of slip, of the *M*5.2 and October 9 *M*4.3 events. Red quadrants in beach ball are compressional first arrivals of seismic waves. The *M*4.3 event was recorded at the portable (LIQ) and permanent accelerographs (HWR, LPA, and OLA) and was used to estimate ground motion at LIQ during the October 3 event.

(Fig. 1). The swarm lies within the Walker Lane Belt, a 100-km-wide zone of active crustal deformation characterized by both mainshock–aftershock sequences and swarm activity (Hauksson and Unruh, 2007). Geodetically determined crustal deformation consists of oblique extension with a right-lateral shear component of ~5.9 mm/year along the southern part of the Owens Valley Fault Zone (McCaffrey, 2005). Rupture of part of the fault zone in 1872, which is ~9 km west of the swarm, caused one of the largest earthquakes ($M$~7.6) in California history (Ellsworth, 1990; Slemmons et al., 2008) (Fig. 1). The earthquake swarm started gradually in April 2009, with 11 events of $M \geq 1.3$ preceding an $M$4.7 event on May 23. The $M$4.7 event was followed by 165 aftershocks of $M \geq 1.3$ that formed a northwest striking aftershock distribution. The sequence resumed on October 1 with a $M$5.0 event followed by a $M$5.2 on October 3 (Fig. 1), and seven $M$~4 events. The latter events included an $M$4.3 on October 9 (Fig. 1), which was recorded on a portable seismic network that we deployed in the liquefaction area. The part of the sequence after October 1, with 570 events of $M \geq 1.3$, occurred at depths ranging from 3 to 10 km, and formed a parallel northwest trend, located 2.5 km to the west of the trend in May, near the northwest striking Centennial Flat Fault (Jayko, 2009) (Fig. 1). No surface rupture was observed along the fault. In addition, some aftershocks of the $M$5.2 earthquake formed a northeast trend of cross faulting that was orthogonal to the two primary northwest trends of seismicity. Fault plane solutions of the $M$>4 events exhibited pure strike–slip faulting on northwest striking or northeast striking nodal planes, consistent with the aftershock trends.

## 3. Liquefaction

Liquefaction during the Olancha $M$5.2 earthquake occurred at the southeast margin of the former Owens Lake (Fig. 1). The area is now a salt flat or playa as the result of diversion during the last century of the Owens River and Sierra Nevada streams into the Los Angeles Aqueduct. We observed liquefaction features along the margin of the playa in an area where an active alluvial fan is depositing coarser grained sediment over fine-grained lake beds. Liquefaction features included ground cracks and sand boils ranging in diameter from meter-size to centimeter- to millimeter-size (Fig. 2). Liquefaction was irregularly distributed within an approximately 2-km-long and 0.6-km-wide N10E trending zone. The epicentral distance from the $M$5.2 earthquake to the liquefaction zone ranged from 2.7 to 3.9 km. We note that the maximum distance of liquefaction to the seismic source, ~3.9 km, lies on the boundary of the curve proposed by Ambraseys (1988, Fig. 67). One of the authors (Jayko) first inspected the liquefaction zone 17 h after the $M$5.2 earthquake and most of the sand boils were still wet and appeared fresh, indicating that they were caused by the $M$5.2 event. Jayko observed a few drier, salt-crusted, and buried sand boils that may have been associated with the $M$5.0 event that occurred 56 h earlier on October 1.

Our field investigation focused on a 0.5-km-long subarea in the southern part of the liquefaction zone where cracks showed a preferred orientation that we interpret to be caused by lateral spreading, i.e., permanent horizontal ground deformation. The predominant orientation of the ground cracks within the subarea was N15°E, with orientations ranging from N15°W to N20°E. Most of the cracks exhibited extension with openings ranging from 1 to 4 cm, and were parallel to slope contours suggesting a downslope movement. The gradient of the topographic slope in the subarea is 3%. Lengths of ground cracks ranged from 2 to 20 m. We also observed a 2- to 3-m-wide graben in the subarea with vertical offsets of 2 to 3 cm across its bounding ground cracks (Fig. 2B). Aggregate extension across the head of the lateral spread is unknown, and no toe or zone of compression was observed.

## 4. Ground motion estimation

We estimated ground motion in the subarea during the $M$5.2 event based on a recording of the October 9 $M$4.3 event with the portable accelerograph (LIQ) (Fig. 1). LIQ was deployed after the liquefaction was observed. Estimation was necessary because the closest permanent accelerograph, OLA, was 18 km from the liquefaction zone (Fig. 1). LIQ was deployed on October 8 at the same location where we subsequently conducted subsurface exploration, approximately 3.7 km southwest of the epicenter of the $M$5.2 event. Ground motion at LIQ was estimated for the $M$5.2 event by scaling peak values recorded for the $M$4.3 aftershock by the ratio of similar peak values recorded for the $M$5.2 mainshock and $M$4.3 aftershock at three permanent accelerographs. The three accelerographs, OLA, LPA, and HWR, were between 18 and 33 km away (Fig. 1). Ratios of peak values for the mainshock to the aftershock of the vector component of horizontal peak ground acceleration (PGA) ranged from 2.37 to 4.34. Multiplying PGA recorded at LIQ during the $M$4.3 aftershock, 0.073 g, by the ratios at the three permanent stations yields an average of PGA = 0.23 g, and a range of 0.17 to 0.32 g for the $M$5.2 event. PGA is consistent with a recent ground motion prediction equation for western United States earthquakes (Boore and Atkinson, 2008). The equation predicts a median of PGA = 0.20 g for a $M$5.2 earthquake at 3.7 km and an average 30-m-deep shear-wave site velocity of 200 m/s; PGA at one standard deviation ranges from 0.12 to 0.32 g.

Our approach for estimating PGA assumes fault plane solutions and the propagation paths to the permanent accelerographs are similar for the mainshock and the aftershock; the ratio is an estimate of the ratio of their source strengths. We feel that the assumption is valid because the epicenters of the $M$4.3and $M$5.2 events were only 0.6 km apart and the earthquakes had comparable fault plane solutions (Fig. 1). In addition, the $M$4.3 had a focal depth of 9.2 km as compared to 9.0 km for the $M$5.2.

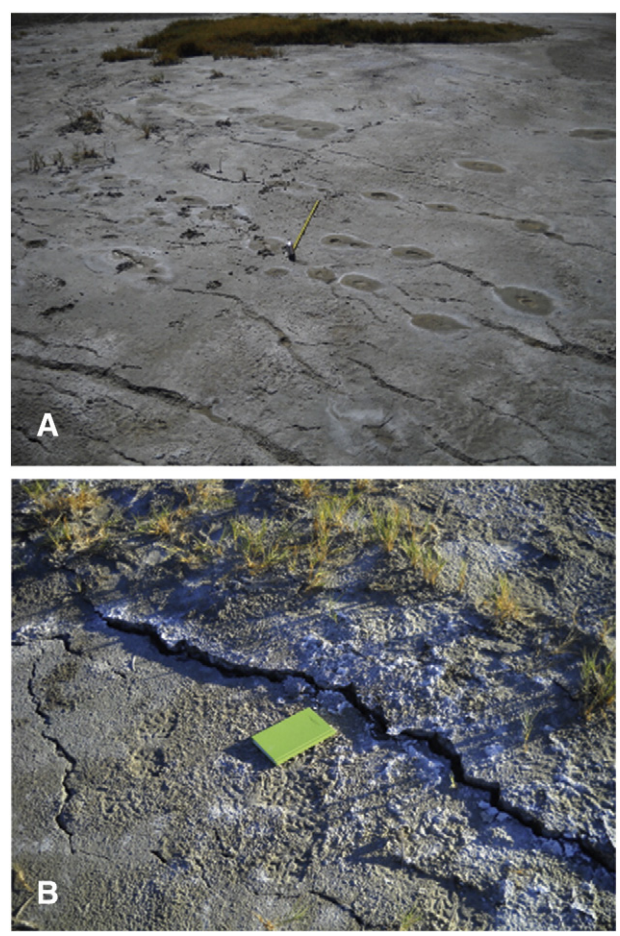


**Fig. 2.** Photographs of liquefaction features. (A) Small sand boils caused by eruptions of liquefied soil. Note alignment along ground cracks. Tape measure scale is 91 cm (B) Ground crack with vertical offset of 3 to 4 cm (notebook is 13 × 20 cm).

## 5. Subsurface exploration

We measured geotechnical properties of soil to a depth of 2.0 m next to the portable accelerograph site LIQ. Grain-size distributions were determined for soil samples that were collected with two hand auger borings, B10 and B12, and with a hammer driven core sampler at B10 (Fig. 3B). We also measured in situ peak and residual resistances with a field vane that was inserted into each open auger hole before sampling (Fig. 3A). Soft ground conditions in the liquefaction area prevented access of our truck-mounted geotechnical exploration system.

The soil samples indicate that the surficial geology consists of a thin cover of fluvial wash and beach sand deposits that overlie fine-grained lake sediment. The uppermost 0.5 to 0.9 m consists of brown pebble- to medium-grained bedded wash deposits. The sediment in the interval of 0.9 to 1.6 m is a gray silty sand beach deposit. The average fines content of the gray sand layer is 13.8 ± 6.7%. The sediment below approximately 1.6 m is a dark greenish gray, very plastic, soft clayey silt with 28% of the particle sizes smaller than 5 μm.

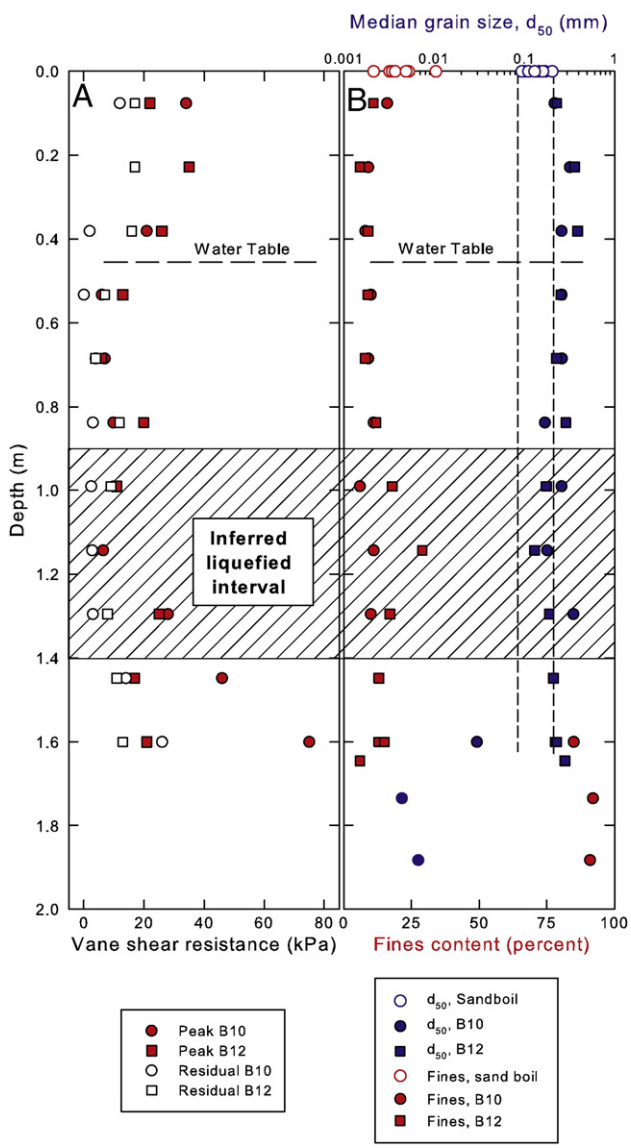


**Fig. 3.** Vertical profile of soil properties at site LIQ (see Fig. 1) based on samples from borings B10 and B12 and coring. (A) In situ peak and residual vane shear resistances. (B) Median-diameter grain size and fines content (percentage with diameter less than 0.075 mm). Soil properties of sand boils are plotted at the surface. Depth interval from 0.9 to 1.4 m is inferred to have liquefied.

The water table in the borings was 0.46 m deep, which is near the base of the fluvial wash deposits. The shallow water table is probably a permanent condition. Active springs discharge at numerous locations near the historic lake shoreline along the southern edge of the playa.

We infer that gray sand from 0.9 to 1.4 m liquefied. First the sand boils were predominantly gray colored. Second, median diameter grain sizes ($d_{50}$) of sand boil samples, 0.144 mm, overlap with median grain sizes in this depth interval, 0.131–0.350 mm (Fig. 3B). Third, vane shear measurements indicate that the weakest and loosest sand in the soil column is between 0.9 and 1.4 m (Fig. 3A). Peak and residual vane shear resistances, respectively, are 14.6 ± 11.3 and 5.1 ± 3.2 kPa. Fourth, the sediment in this interval is fine-grained sand to silty sand with fines (<0.075 mm) contents of 15.2 ± 8.1%. This sediment favorably compares to liquefiable sands at other liquefaction sites (International Navigation Association, 2001). And fifth, the inferred shallow source depth is consistent with the small diameter (<100 mm) of many sand boils and the absence of field evidence such as splatter from highly pressurized ejecta. Both field observations suggest that liquefaction-induced pore-water pressure was low and of short duration when the soil liquefied. When a soil strata liquefy, pore-water pressure rises to the total overburden stress (Holzer and Youd, 2007). Thus, the shallower the liquefaction, the lower the water pressure and head that drives the venting water and slurry that create the sand boils.

## 6. Liquefaction potential analysis

Because reports of liquefaction at small earthquake magnitudes are rare, we tested how well the internationally used Seed–Idriss simplified procedure (Seed and Idriss, 1971) predicted the Olancha liquefaction. We used the popular National Center for Earthquake Engineering Research (NCEER) version of the procedure for the analysis (Youd et al., 2001). This standardized engineering procedure relies on field penetration tests to evaluate liquefaction potential. In the procedure, penetration resistance and seismic loading are plotted on a chart and compared to the liquefaction strength of sandy soil that is based on many case histories (Youd et al., 2001). The standard penetration test (SPT) is the most common field penetration test used in engineering practice to assess liquefaction potential. In the SPT, a standardized soil sampler is hammered into the soil and the number of blows required to advance the sampler one foot is counted. The field blow count is normalized for stress and corrected for a variety of factors (Idriss and Boulanger, 2008).

We inferred blow counts from residual vane shear resistance because as noted we could not drive our geotechnical exploration system into the study area and measure penetration resistance. We assumed that residual vane shear resistance in the sand approximates residual shear strength, and used a recent correlation of residual strength with SPT blow counts (Idriss and Boulanger, 2008). The average residual vane shear resistance in the inferred liquefaction interval, 5.1 kPa, implies a normalized, corrected, clean-sand-equivalent blow count [$(N_1)_{60CS}$] of 5 blows/ft; residual vane shear resistances at one standard deviation, 1.9 and 8.3 kPa, imply blow counts ranging from 3.5 to 8.0 blows/ft, respectively. These inferred low blow counts are consistent with our field observation that the shear vane tended to fall into the sand under its own weight upon being lowered into the hole. In our experience, sands that cannot support even modest field loads generally have low field blow counts, typically ~2 blows/ft or less. A field blow count of 2 blows/ft with a fines content of 15.2% yields an $(N_1)_{60CS}$ of 6.7 blows/ft.

The simplified procedure predicts soil should have liquefied in the 0.9- to 1.4-m depth interval at LIQ during the *M*5.2 Olancha earthquake (Fig. 4). In Fig. 4, the ordinate is the cyclic stress ratio, which is an average seismic load computed from PGA and vertical effective stress; the abscissa is the normalized, corrected, clean-sand-equivalent blow count (Youd et al., 2001). The simplified procedure is referenced to a *M*7.5 earthquake, and a magnitude scaling factor

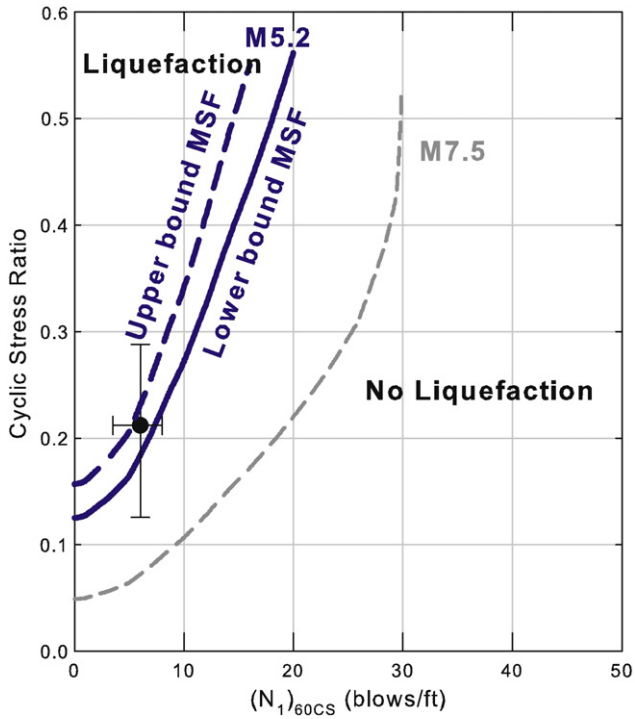


**Fig. 4.** Prediction of liquefaction potential of silty sand in the 0.9 to 1.4 m depth interval at LIQ based on the NCEER version of the Seed–Idriss simplified procedure (Youd et al., 2001). Cyclic stress ratio measures strength of earthquake shaking; blow count is a function of soil density. Normalized, corrected, clean-sand-equivalent blow count, $(N_1)_{60CS}$, was inferred from residual shear resistance. Boundary curves for an *M*5.2 earthquake are shown for both lower and upper bound MSFs recommended by the NCEER version.

(MSF) is used to adjust for different magnitudes. We computed the *M*5.2 liquefaction boundary curve with both the lower and upper bound MSFs recommended by the NCEER version (Youd et al., 2001). The lower bound MSF produces a more conservative prediction than does the upper bound MSF, and is therefore more commonly used in engineering practice. The prediction of liquefaction potential at LIQ with the upper bound MSF is more ambiguous, but the proximity of the observed point to the boundary curve would prompt additional investigation in most applications of the simplified procedure.

## 7. Conclusions

Liquefaction and lateral spreading during the Olancha *M*5.2 earthquake provided a rare opportunity to investigate the factors that contribute to liquefaction during small magnitude earthquakes. Liquefaction during small magnitude earthquakes presumably depends on the presence of either or both very susceptible soil and anomalously high ground motion. We conclude that the liquefaction was a consequence of site conditions and did not result from anomalously large ground motion. Both the shallow water table and the presence of shallow very liquefiable sands were the primary factors that contributed to the liquefaction. Field-based estimates of PGA were near median values of western United States *M*5.2 earthquakes.

For engineering practice, successful prediction of the Olancha earthquake liquefaction with the Seed–Idriss simplified procedure is encouraging. Although only a single case history, the procedure worked for a much smaller earthquake than those in the case history database on which the procedure is based.

For earthquake geology, the shallowness (<2 m) of the deposits that liquefied, i.e., the source beds, may provide criteria for potentially recognizing when paleoliquefaction features may have been caused by small earthquakes, although documentation in additional small earthquakes is needed. The associated source beds of the paleoliquefaction features should be observable in most trenches and outcrops, which usually extend to 2-m depths. Shallow source beds for liquefaction features do not preclude larger earthquakes, but are at least consistent with small magnitude earthquakes. In any case, our study, when combined with the other observations of liquefaction during small earthquakes, indicates that paleoliquefaction features need not imply either large earthquake magnitude or large ground motion.

## Acknowledgments

We thank Grace A. McCarley-Holder and Earl Wilson of the Great Basin Unified Air Pollution Control District for help with logistics and sampling; Ross W. Boulanger, Wayne R. Thatcher, and John C. Tinsley, III, for constructive reviews; Coyn C. Criley for the grain-size analyses; and Hamid Haddadi and Christopher D. Stephens for help in retrieving the permanent accelerograph records.

## References

Ambraseys, N., 1988. Engineering seismology. Earthquake Engineering and Structural Dynamics 17 (1), 1–105.
Boore, D.M., Atkinson, G.M., 2008. Ground-motion prediction equations for the average horizontal component of PGA, PGV, and 5 %-damped PSA at spectral periods between 0.01 s and 10.0 s. Earthquake Spectra 24 (1), 99–138.
Cetin, K.O., Seed, R.B., Kiureghian, A.D., Tokimatsu, K., Harder, L.F., Kayen, R.E., Moss, R.E.S., 2004. Standard penetration test-based probabilistic and deterministic assessment of seismic soil liquefaction potential. Journal of Geotechnical and Geoenvironmental Engineering 130 (12), 1314–1340.
Ellsworth, W.L., 1990. Earthquake history, 1769-1989. In: Wallace, R.E. (Ed.), The San Andreas Fault system: Professional Paper 1515, U.S. Geological Survey, pp. 153–181.
Galli, P., 2000. New empirical relationships between magnitude and distance for liquefaction. Tectonophysics 324 (3), 169–187.
Hauksson, E., Unruh, J., 2007. Regional tectonics of the Coso geothermal area along the intracontinental plate boundary in central eastern California: three-dimensional Vp and Vp/Vs models, spatial-temporal seismicity patterns, and seismogenic deformation. Journal of Geophysical Research 112 B06309-B00633.
Holzer, T.L., Youd, T.L., 2007. Liquefaction, ground oscillation, and soil deformation at the Wildlife Liquefaction Array. Seismological Society of America Bulletin 97 (3), 961–976.
Idriss, I.M., Boulanger, R.W., 2008. Soil liquefaction during earthquakes. EERI Monograph MNO-12, Oakland, CA, USA.
International Navigation Association, 2001. Seismic Design Guidelines for Port Structures. A. A. Balkema Publishers, Tokyo, Japan.
Jayko, A.S., 2009. Surficial geology of the Darwin Hills 30' X 60' Quadrangle, Inyo County, California. Scientific Investigations Map 3040, U.S. Geological Survey.
Kuribayashi, E., Tatsuoka, F., 1975. Brief review of liquefaction during earthquakes in Japan. Soils and Foundations 15 (4), 81–92.
McCaffrey, R., 2005. Block kinematics of the Pacific–North America plate boundary in the southwestern United States from inversion of GPS, seismological, and geologic data. Journal of Geophysical Research 110, B07401–B07427.
Moss, R.E.S., Seed, R.B., Kayen, R.E., Stewart, J.P., Kiureghian, A.D., Cetin, K., 2006. CPT-based probabilistic and deterministic assessment of in situ seismic soil liquefaction potential. Journal of Geotechnical and Geoenvironmental Engineering 132 (8), 1032–1051.
Obermeier, S.F., Olson, S.M., Green, R.A., 2005. Field occurrences of liquefaction-induced features: a primer for engineering geologic analysis of paleoseismic shaking. Engineering Geology 76 (3–4), 209–234.
Seed, H.B., Idriss, I.M., 1971. Simplified procedure for evaluating soil liquefaction potential. Journal of Soil Mechanics and Foundation Engineering 97 (9), 1249–1273.
Sims, J.D., Garvin, C.D., 1995. Recurrent liquefaction induced by the 1989 Loma Prieta earthquake and 1990 and 1991 aftershocks: implications for paleoseismicity studies. Seismological Society of America Bulletin 85 (1), 51–65.
Slemmons, D.B., Vittori, E., Jayko, A.S., Carver, G.A., Bacon, S.N., 2008. Quaternary Fault and Lineament Map of Owens Valley, Inyo County, Eastern California. Map and Chart Series 96. Geological Society of America.
Youd, T.L., Idriss, I.M., Andrus, R.D., Arango, I., Castro, G., Christian, J.T., Dobry, R., Finn, W.D.L., Harder Jr., L.F., Hynes, M.E., Ishihara, K., Koester, J.P., Liao, S.S.C., Marcuson III, W.F., Martin, G.R., Mitchell, J.K., Moriwaki, Y., Power, M.S., Robertson, P.K., Seed, R.B., Stokoe II, K.H., 2001. Liquefaction resistance of soils: summary report from the 1996 NCEER and 1998 NCEER/NSF workshops on evaluation of liquefaction resistance of soils. Journal of Geotechnical and Geoenvironmental Engineering 127 (10), 817–833.
Youd, T.L., Hansen, C.M., Bartlett, S.F., 2002. Revised MLR equations for prediction of lateral spread displacement. Journal of Geotechnical and Geoenvironmental Engineering 128 (12), 1007–1017.